Templated Crystallization from Oriented Gyroid and Hexagonal Melt Phases in a Diblock Copolymer

I. W. Hamley,*,† V. Castelletto,† G. Floudas,‡ and F. Schipper§

Department of Chemistry, University of Leeds, Leeds LS2 9JT, UK; Department of Physics, University of Ioannina, 45 110 Ioannina, Greece, and Institute of Biomedical Research (IBR-FORTH), Ioannina, Greece; and Foundation for Research and Technology-Hellas, I.E.S.L., 711 10 Heraklion, Crete, Greece

Received May 6, 2002; Revised Manuscript Received July 30, 2002

ABSTRACT: Crystallization from oriented hexagonal-packed cylinder (hex) and gyroid (gyr) melt phases in an asymmetric poly(ethylene oxide)-*b*-poly(isoprene) diblock copolymer is investigated by small-angle X-ray scattering with simultaneous rheology. Crystallization from a shear-oriented hex phase leads to crystalline lamellar planes parallel to the cylinders and a step increase in domain spacing. Crystallization from an oriented gyroid crystal, grown from a shear-aligned hex phase, is templated by the {220} lattice planes, leading to an oriented crystalline lamellar phase. The domain spacing increases by 40% on crystallization, indicating a transition that is strictly not epitaxial, although crystallographic register between lattice planes is maintained. The orientation of the lamellar crystal structure is compared to that recently observed for a poly(oxybutylene)-*b*-poly(oxyethylene) diblock crystallized from an aligned gyroid phase.

1. Introduction

The templating of hard materials by soft materials is currently attracting considerable attention.[1] Semicrystalline block copolymers can act as model systems for this process because the "soft" structure formed in a block copolymer melt can template the formation of a "hard" semicrystalline structure.[2] The templating requires that crystallographic register between the orientation of lattice planes in the melt phase and crystal phase be conserved; however, the length scale of the microstructure can change (crystallization can cause a discontinuous increase in domain spacing). In this case, the transformation between two phases must be distinguished from an *epitaxial* transition, in which crystallographic register between lattice planes is retained and the domain spacing changes continuously across the transition. Epitaxial relationships are now well-known for block copolymer melts, involving transitions between two phases among the equilibrium structures: lamellar (lam), hexagonal (hex), gyroid (gyr), and body-centered-cubic (bcc) structures.[3] However, there has been less work on phase transitions from oriented melt phases to crystal phases in block copolymers. The present study concerns the transition between the hexagonal and gyroid melt phases and the semicrystalline lamellar (lam_c) structure.

A number of previous studies have focused on crystallization in semicrystalline block copolymers, starting from an oriented melt structure.[2,4−18] If the crystallization temperature (T_c) is below the glass transition temperature of the amorphous block, it is found that crystallization is confined by the glassy domain.[7,8,11−18] In the case of block copolymers in which the noncrystalline block is rubbery ($T_c > T_g$), formation of a lamellar crystal structure can overwhelm the precursor melt structure (depending also on cooling rate[19,20]), if the block copolymer is weakly segregated.[7−9,19,21−23] However, if the copolymer is sufficiently strongly segregated, crystallization can be guided by[19,24] or entirely confined within[10,11,23] the melt microdomains (cylinders[11] or spheres[10]). Morphology changes upon crystallization in block copolymers have been the focus of a recent review.[4]

In this paper, we present results from simultaneous SAXS/rheology experiments on the formation of an oriented lamellar crystalline phase on cooling from oriented gyr or hex melt phases in a diblock copolymer. The alignment of planes of cylinders in a shear-oriented hexagonal phase templates the orientation of lamellar planes in the lam_c phase. Similarly, an aligned gyroid phase templates the crystallization in the lam_c phase, the orientation of which matches that of the {220} planes of the gyroid structure. Crystallization from the oriented gyr melt phase of a poly(butylene oxide)-*b*-poly(ethylene oxide) (PBO−PEO) diblock has been investigated via small-angle X-ray scattering.[2] Crystallization of PEO led to a lamellar structure with an approximate doubling of domain spacing. However, crystallographic register was maintained between lamellar planes and a subset of the set of {211} planes of the gyroid structure, which was shear oriented such that a [111] direction coincided with the shear direction, forming a directionally oriented[25] crystal. The selection of specific {211} planes was ascribed to symmetry breaking imposed by the temperature gradient from the outside of the shear tools to the inside (coincident with the shear gradient direction in the melt).[2] Epitaxial relationships have been observed on melting a crystalline lamellar polyolefin diblock (to form a hex structure)[7] and on cooling a hex phase in a poly(ethylene oxide)-containing diblock.[26]

Our poly(ethylene oxide)-*b*-poly(isoprene) (PEO−PI) diblock copolymer has been the subject of recent investigations.[27−29] The phase diagram[29] consists of four equilibrium phases in the melt: lam, hex, bcc, and gyr. The latter is formed for a range of PEO volume frac-

† University of Leeds.
‡ University of Ioannina and IBR-FORTH.
§ Foundation for Research and Technology-Hellas.
* Author for correspondence.

10.1021/ma0207069 CCC: $22.00
Published on Web 10/05/2002

tions: $0.39 < f_{PEO} < 0.45$ and $0.66 < f_{PEO} < 0.7$. Order-to-order transitions in the *unoriented* state have been the subject of a previous letter,[28] in which the kinetics of the hexagonal to the gyroid phase transformation were investigated as well as other order−order phase transitions (including those to and from the crystalline lamellar phase) by time-resolved SAXS. The hexagonal-to-gyroid transformation was found to proceed via a nucleation and growth mechanism with a small mismatch (less than 2%) in domain spacing between the two phases. In the present investigation we employ the copolymer PEO−PI 4−5 with $f_{PEO} = 0.39$ and study the crystallization from *oriented* hexagonal and gyroid phases.

2. Experimental Section

Synthesis. The diblock copolymer (coded PEO−PI 4−5) was prepared via anionic polymerization, as described in detail elsewhere.[27] The number-averaged molecular weights of PEO and PI were 4400 and 5400, respectively, and the polydispersity index ($\bar{M}_w/\bar{M}_n$) was 1.08. Based on the densities for PI and PEO (0.895 and 1.12 g/cm^3, respectively), the PEO volume fraction is $f_{PEO} = 0.39$. Despite the low molecular weight, the diblock exhibits ordered phases due to the high incompatibility between the two blocks, which leads to χN ($T = 25$ °C) = 62, using the published χ parameter for PI−PEO diblocks.[27,29]

SAXS/Rheology. Small-angle X-ray scattering experiments with simultaneous rheology were conducted at the Synchrotron Radiation Source, Daresbury Laboratory, UK, on beamlines 2.1 and 16.1. Both beamlines are configured for SAXS experiments using monochromatic radiation of wavelength $\lambda = 1.5$ Å. Details of the beamlines and data collection electronics have been given elsewhere.[30,31] The diffraction pattern was collected on a multiwire gas-filled area detector. A scattering pattern from a specimen of wet collagen (rat-tail tendon) was used for calibration of the q scale ($q = (4\pi/\lambda) \sin\theta$, where the scattering angle is 2θ).

Samples were subjected to oscillatory shear using a modified strain-controlled rheometer (Rheometrics RSA II) with a shear sandwich geometry. A detailed description of this instrument, modified to enable simultaneous SAXS/rheology experiments, is provided elsewhere.[32,33] Briefly, the shear sandwich cell comprises three rectangular plates, the two external plates being fixed while the central piece oscillates vertically. The sample is soft above the PEO melting temperature, and it was loaded on both sides symmetrically about the insert piece. Apertures were machined into the plates of the shear sandwich assembly to allow transmission of the X-ray beam and were covered by Kapton polyimide windows. The shear sandwich plates are perpendicular to the X-ray beam, which is incident along the shear gradient direction $\nabla\mathbf{v}$, so that the ($\mathbf{v}$,$\mathbf{e}$) plane is accessed in SAXS experiments ($\mathbf{v}$ is the shear direction; $\mathbf{e}$ is the neutral direction). The shear frequency is denoted ω and the strain amplitude γ.

Crystallization experiments were performed by quenching the samples from the melt to room temperature by opening the oven doors on the rheometer. This was found to provide faster cooling than attempting to cool the (relatively large thermal mass) oven using the liquid nitrogen cooler attachment. Separate experiments in which samples were quenched by pouring liquid nitrogen on them produced similar results to those reported here.

3. Results and Discussion

3.1. Phase Behavior. Equilibrium phase transitions in PEO−PI 4−5 were investigated by DSC, rheology, and SAXS, as described previously.[28] Figure 1 presents data from differential scanning calorimetry (DSC) and rheology experiments during a heating ramp. DSC reveals a strong endothermic peak at about 52 °C associated with melting of the lam$_c$ phase (with a latent heat ΔH_f of 56 J/g resulting in a PEO crystallinity of 75%). Two endothermic peaks at about 125 and 225 °C, which have much smaller latent heats, 0.3 and 0.4 J/g, respectively, could also be detected. The latter value corresponds to that expected for the order-to-disorder transition (ODT). An isochronal temperature ramp of the dynamic elastic storage modulus (Figure 1) indicates changes in elasticity at about the same temperatures. The corresponding structures were identified via SAXS on unaligned samples.[28] The low-temperature phase with the highest modulus (lam$_c$) melts to a hex phase that then transforms to the gyr phase, for which G' is larger because it is a three-dimensional periodic structure (solid) rather than a two-dimensional hex phase. At about 225 °C the gyroid melts to the disordered phase. Having established the phase boundaries, SAXS experiments were conducted to investigate the orientation of the crystalline morphology, starting from aligned melt phases. The hex phase was aligned by large-amplitude oscillatory shear. An aligned gyroid crystal was grown from a shear-oriented hex phase precursor.

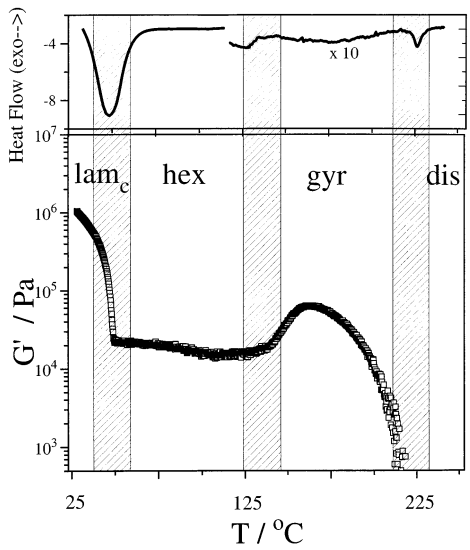

Figure 1. Top: differential scanning calorimetry data (heating rate 1 °C/min). Bottom: temperature dependence of the isochronal ($\omega = 1$ rad/s, $\gamma = 0.5\%$) dynamic storage modulus obtained during a heating ramp.[28]

3.2. Crystallization from the Shear-Aligned Hexagonal Phase. SAXS patterns for the hex phase before and after shear at $T = 90$ °C are shown in parts a and b of Figure 2, respectively. Prior to shear the sample is unoriented. However, following large-amplitude oscillatory shear ($\omega = 100$ rad/s, $\gamma = 70\%$) for 6 min, a high degree of alignment is obtained. The SAXS intensity is concentrated on the equator, consistent with orientation of cylinders parallel to the (vertical) shear direction. Confirmation of a hexagonal structure is provided by the presence of higher-order reflections. These are apparent in the radially averaged data shown in Figure 3. Strong reflections are observed at q^*, $2q^*$, and $\sqrt{7}q^*$ and a weak peak at $\sqrt{3}q^*$ can just be discerned. The strong reflections at q^* and $2q^*$ indicate orientation of planes of cylinders in the ($\mathbf{v}$,$\nabla\mathbf{v}$) plane, although the presence of the other two weak reflections suggests a slight degree of misorientation about the cylinder axis.[34,35]

Starting from the oriented hex phase, the sample was quenched to room temperature, where crystallization was completed after approximately 10 min, as shown

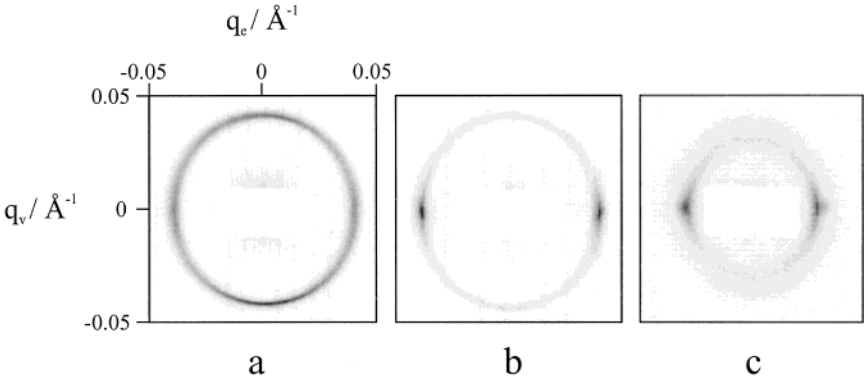

Figure 2. SAXS patterns obtained using the SAXS rheometer (the shear direction is vertical). (a) In the hex phase at $T = 90$ °C, prior to shearing. (b) In the hex phase at $T = 90$ °C following 6 min of shear at $\omega = 100$ rad/s, $\gamma = 70\%$. (c) In the lam_c phase at room temperature (30 min after quenching from hex phase).

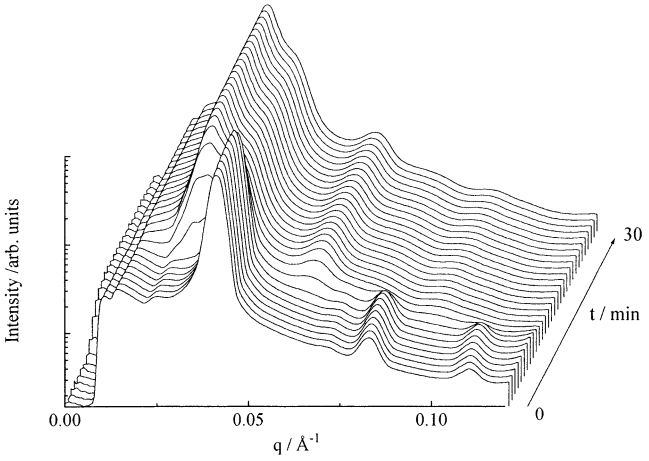

Figure 3. Profiles of SAXS data reduced to intensity vs wavenumber as a function of time during isothermal crystallization at $T \approx 25$ °C, following a quench from the hex phase. The transition from hex to lam_c occurs at around $t = 10$ min.

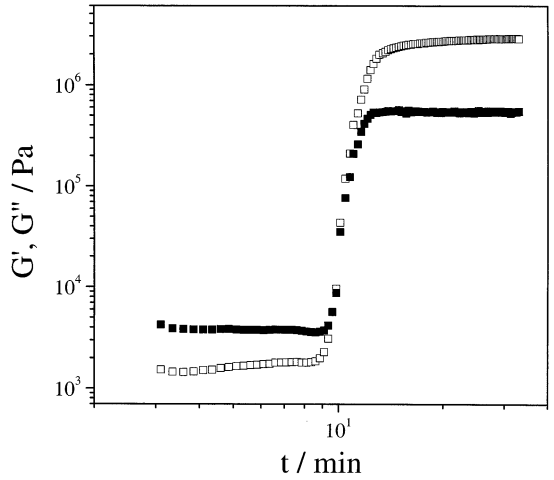

Figure 4. Growth of the dynamic shear moduli following a temperature quench from $T = 90$ °C to $T \approx 25$ °C ($\omega = 1$ rad/s, $\gamma = 2\%$): (□) storage modulus, (■) loss modulus. Time $t = 0$ is defined as the time at which room temperature was reached.

by SAXS (Figure 3) and rheology (Figure 4) obtained concurrently. The SAXS pattern obtained after 30 min is shown in Figure 2c. It is apparent that crystallization has been templated by the aligned hexagonal phase, since despite the change in length scale of the structure, the equatorial orientation of peaks in the SAXS patterns is maintained. Crystallization occurred with a significant, and discontinuous, change in domain spacing: From $q^* = 0.043 \pm 0.0005$ Å^{-1} in the hex phase to $q^* = 0.032 \pm 0.0005$ Å^{-1} in the lam_c phase, the latter corresponding to a lamellar domain spacing $d = 203 \pm 4$ Å, in accordance with an earlier investigation on an unaligned sample.[28] In an earlier study[28] we found long incubation times (~700 s) followed by the nucleation and growth of the lam_c at the expense of the hex phase. Likewise in the present case, there is long-time coexistence of the two phases as indicated by the presence of mixed reflections in Figure 3. The common orientation of planes of cylinders and lamellae for this transition indicates crystallographic register, despite the jump in length scale on crystallization which means that the transformation does not occur epitaxially. Instead, the soft hex phase provides a template for crystallization to occur at a larger length scale.

3.3. Crystallization from an Aligned Gyroid Phase. The gyroid phase cannot usually be aligned by applying shear, which disrupts the bicontinuous structure.[36] Instead, an oriented gyroid crystal can be grown epitaxially by shearing in an adjacent lam or hex phase.[25,37,38] Here, an oriented gyroid crystal was grown from a shear-oriented hex phase. The starting point at $T = 90$ °C was characterized by a SAXS pattern similar to Figure 2b, with strong equatorial reflections from planes of cylinders aligned along the shear direction. The sample was then rapidly heated (in less than 5 min) to 160 °C, at which temperature a SAXS pattern from a well-aligned gyroid crystal was observed to develop over 15 min. The SAXS pattern obtained after this equilibration period is shown in Figure 5a. This "10-spot" pattern from the gyroid phase (space group $Ia\bar{3}d$) has been analyzed elsewhere.[25,38] It corresponds to a directionally oriented crystal in which a [111] direction lies along the shear direction. (For convenience in the subsequent discussion, the indexation of the pattern previously reported is reproduced in Figure 8.) The SAXS patterns previously observed[25,38] contain two equatorial reflections, along with two pairs offset from the equator by ±28.1°. An additional set of four reflections are located at ±19.5° with respect to the vertical. The angles measured from an azimuthal scan centered on q^* shown in Figure 6 are consistent with these values. The orientation of 220 peaks can also be quantified from the azimuthal scan shown in Figure 6. In addition to the equatorial reflections, two pairs of peaks can be identified, close to the angle ±54.7° (with respect to the equator) expected for this oriented gyroid pattern.[25] Further confirmation of a gyroid structure is

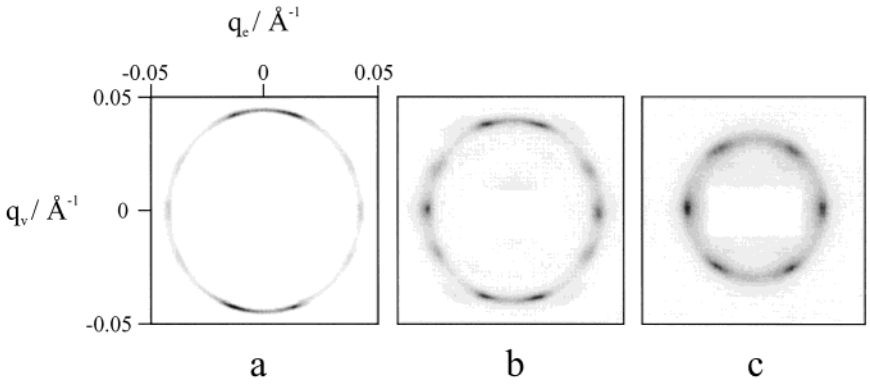

Figure 5. SAXS patterns obtained using the SAXS rheometer (the shear direction is vertical). (a) In the gyr phase at $T = 160$ °C, following growth from a shear-aligned hex phase. (b) Supercooled gyr phase at $T \approx 25$ °C. Recorded 2 min after the quench from $T = 160$ °C. (c) In the lam$_c$ phase at $T \approx 25$ °C (30 min after quenching from the gyr phase).

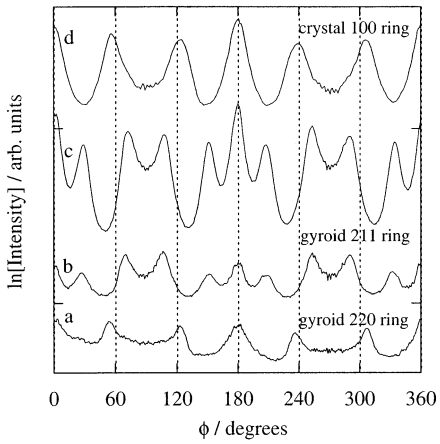

Figure 6. Azimuthal variation of SAXS intensity (angle ϕ defined with respect to the horizontal) in a narrow band containing the diffraction rings indicated: (a) gyr 220 ring ($T = 160$ °C), obtained from pattern in Figure 5a; (b) gyr 211 ring ($T = 160$ °C), obtained from pattern in Figure 5a; (c) gyr 211 ring, obtained from pattern in Figure 5b (supercooled gyr); (d) lam$_c$ 100 ring ($T \approx 25$ °C), obtained from pattern in Figure 5c.

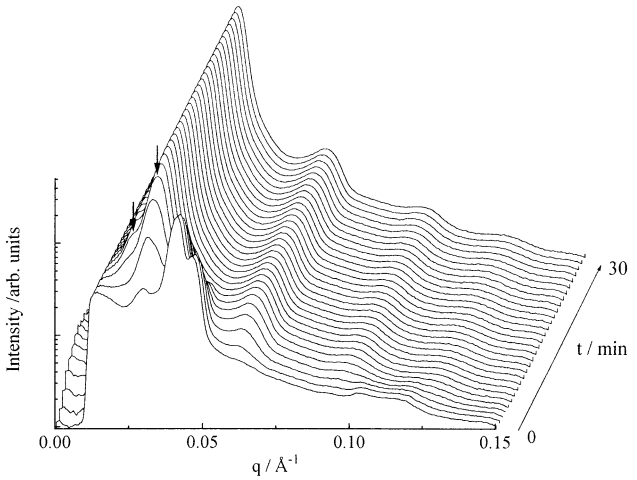

Figure 7. Profiles of SAXS data reduced to intensity vs wavenumber as a function of time during isothermal crystallization at $T \approx 25$ °C, following a quench from the gyr phase. The transition from gyr to lam$_c$ occurs at around $t = 6$ min. The SAXS peaks corresponding to two populations of lamellar crystals with different thickness (see text) are indicated by arrows.

provided by the presence of reflections at q^*, $1.15q^*$, $1.53q^*$, and other weak higher-order reflections that are not well resolved (Figure 7). These correspond respectively to 211-, 220-, and 321-type reflections of the $Ia\bar{3}d$ space group.

Having grown an oriented gyroid crystal, it was then quenched to room temperature. A SAXS pattern recorded 2 min after the quench is shown in Figure 5b. It shows a supercooled 10-spot pattern from a gyroid phase, with no indication of crystallization at this stage. The supercooling in fact produces a particularly clear oriented SAXS pattern, with many higher orders of reflection (not shown). Crystallization started to occur at room temperature just after 5 min and was complete after 15 min, as shown by the time-dependent shear moduli which indicate a sharp crystallization mechanism as found in homopolymer crystallization under shear.[39] Changes in the morphology were monitored by SAXS. A stacked plot of data reduced to one-dimensional form (by sector averaging) is shown in Figure 7, and a transformation from the gyr to lam$_c$ phase at around the fourth frame is apparent. There is no evidence for a transient hex phase on quenching the gyr phase.

Figure 5 shows that the gyr melt phase templates the orientation of the lam$_c$ crystal, despite the step increase in domain spacing on crystallization, from $q^* = 0.045 \pm 0.0005$ Å^{-1} in the gyroid phase at 160 °C to $q^* = 0.031 \pm 0.0005$ Å^{-1} in the lam$_c$ phase (via $q^* = 0.041 \pm 0.0005$ Å^{-1} in the supercooled gyr phase). The domain spacing in the lam$_c$ phase is the same as that obtained on crystallization from the hex phase. The SAXS pattern for the crystallized sample is shown in Figure 5c. The corresponding azimuthal scan of intensity shown in Figure 6 reveals that the peak maxima are located at the same angles as the 220 peaks in the melt gyroid structure (and supercooled gyroid). Specifically, there is a small but significant deviation of azimuthal angle for the off-equatorial peaks from 60° toward 55° (54.7° expected). A minor proportion of crystals is present with a smaller $q^* = 0.023 \pm 0.0005$ Å^{-1}, characteristic of a larger domain spacing from presumably less-folded PEO crystals. (This peak was observed consistently in repeated quenching experiments.) The orientation of these peaks is identical to that of the strong lam$_c$ peaks. The SAXS peaks corresponding to the two sets of crystal peaks are indicated with arrows in Figure 7.

The crystallization times estimated from the rheology data for the gyroid phase (not shown) cannot be directly compared to those for crystallization of the hex phase discussed in the preceding section, since the experiments were not performed under strict isothermal conditions. In fact, recent measurements of the crystal-

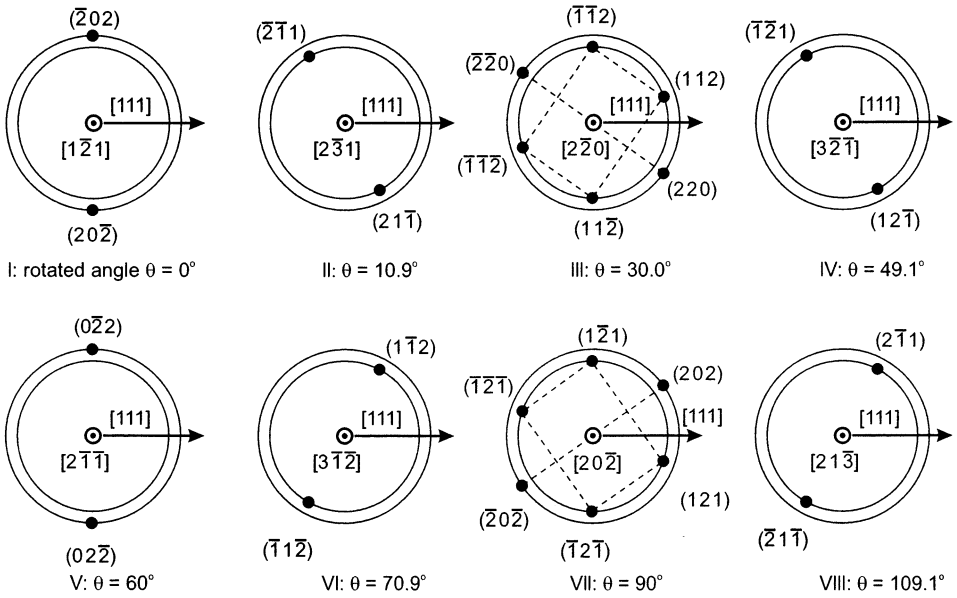

Figure 8. SAXS patterns leading to the "10-spot" pattern of the gyroid phase (Figure 8 from ref 25). Sequence of eight diffraction patterns encountered as the gyroid structure is rotated around the [111] direction. Each pattern corresponds to a planar cut through the reciprocal space. The normals to the cuts are indicated by the end-on arrows. The shear direction is horizontal.

lization kinetics in PEO−PI diblock copolymers under isothermal conditions reveal path-dependent crystallization kinetics, suggesting that the nature of the melt phase exerts a large influence on the crystallization kinetics.[40]

4. Discussion

Our results show some similarities to prior reports, but also some important differences. The breakout crystallization observed in our PI−PEO diblock is distinct from the confined crystallization reported for PS−PEO diblocks[12−18] because PI is rubbery at room temperature, whereas PS is glassy. We can make comparisons however to a prior report[2] on a SAXS study of crystallization from the gyr phase in a PBO−PEO diblock. In common with that work, we observe that the melt gyroid phase templates the orientation of the lamellar crystal, despite a large increase in domain size (doubling in their case, 40% increase in ours). In both cases, breakout crystallization occurs. However, there are subtle differences in the orientation of the templated lam_c phase. We find that the {220} planes of the gyroid phase template the orientation of the lam_c structure. In contrast, Fairclough et al. found, when probing a small sample volume, that the lamellae crystallized in selected {211} planes of the gyroid lattice, suggesting a grain size ∼10 μm. When a larger volume was illuminated by the X-ray beam, several sets of {211} planes were in the diffracting condition. There are several differences in our PI−PEO diblock compared to the PBO−PEO diblock that could help to explain the results, despite the same initial melt state (10-spot gyroid SAXS pattern) and quiescent cooling conditions. The samples are similar in composition; the PBO−PEO diblock contains a volume fraction $f_{PEO} = 0.42$ compared to $f_{PEO} = 0.39$ for our diblock (the number-average molar masses are also similar) so this seems not to be significant. However, the PBO−PEO sample only exhibits a melt gyroid phase, with no lower temperature hex phase. In addition, using the published χ parameter for the PBO−PEO[41] system, we obtain χN (T = 25 °C) = 14, significantly lower than χN (T = 25 °C) = 62 for our sample. The difference in the extent of segregation may have a subtle influence on PEO stem orientation[12,15,17,18] and hence templated lam_c orientation. This requires further detailed wide-angle X-ray scattering experiments.

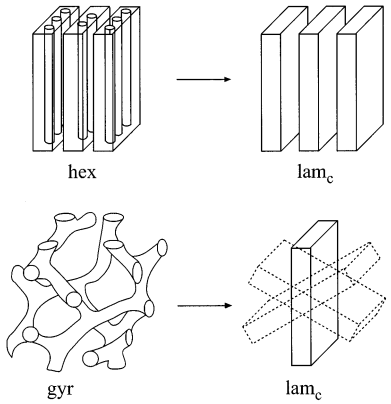

Figure 9. Schematic of phase transformation relationships.

There are however some similarities between our results and those of Fairclough et al. First, a careful inspection of azimuthal intensity profiles for the lam_c phase in their paper (Figure 4) indicates a significant fraction of crystals in registry with the melt 220 peaks. They proposed that crystallization occurred with a thermal gradient along the shear gradient direction, and this symmetry-breaking field selected a [20$\bar{2}$] direction;[25] therefore, crystallization of lamellae occurred with crystallographic register between lamellae and {211} planes of the gyroid containing a [20$\bar{2}$] zone axis (Figure 8, III and VII). In our case, the {220} planes are also accessed when a [20$\bar{2}$] direction is orthogonal to the [111] shear direction. In our case, the stronger segregation of the diblock leads to more intense 220 reflections, which act to template the lamellar crystal orientation.

A schematic of the crystallographic relationships between hex, lam_c, and gyr phases on the basis of our experiments is provided in Figure 9. It is interesting to note that the observed crystallographic relationships are distinct from those usually observed between lam, hex,

and gyr melt or solution phases. Previous reports on block copolymers[25,38] and amphiphile solutions[42,43] have shown an epitaxial relationship between the [111] direction of the gyr phase and hexagonal-packed cylinders and between {211} planes in the gyr phase and lamellar planes. (In the case of block copolymers these may be perforated lamellae.[25,38]) In contrast to these systems, the transition to the lam_c phase in our sample is not epitaxial as there is a large increase in domain spacing. However, the soft cubic structure controls the initial symmetry breaking crystallization step, leading to a templated orientation. That we have observed the same effect for the hex phase adds weight to our interpretation. The retention of orientation with a jump in length scale observed on crystallization suggests a possible mechanism based on crystallization of PEO at the block copolymer interface. The stretching of chains that accompanies crystallization presumably causes the increase in length scale, while the pinning of block junctions to interfaces ensures that crystallographic register between lattice planes is retained. These remarks are as yet qualitative and speculative, and further experiments, for example wide-angle X-ray scattering are required to elucidate stem orientation of PEO chains. The templating of orientation in the gyroid phase is particularly intriguing given that the oriented melt consists of small grains in the directionally oriented crystal. Specific directions for crystallization within grains are selected by two symmetry-breaking directions: the [111] direction selected by shear and [220] directions selected by the thermal gradient.

5. Summary

The formation of a semicrystalline lamellar phase due to crystallization of poly(ethylene oxide) in an asymmetric poly(ethylene oxide-*b*-isoprene) diblock copolymer from shear-oriented melt phases has been investigated via SAXS. We have shown that crystallization is accompanied by an increase in microphase period of ca. 40%. In addition, orientational relationships are maintained between melt phases and the lam_c phase: For crystallization from a hex phase, semicrystalline lamellae were formed from planes of cylinders aligned in the shear plane. The {220} planes in a directionally oriented gyroid template the crystallization of the lam_c phase. The relationship of these results to previously observed epitaxial relationships between gyr and hex or lam phases for block copolymer melts and lyotropic liquid crystals was discussed. The distinction is the length scale jump brought about by the crystallization force, which leads to a non-epitaxial transition. These results provide further information on the templating of hard crystalline phases by soft melt phases in model block copolymer systems.

Acknowledgment. This work was performed within a collaboration supported by the EU-TMR network "Complex Architectures in Diblock Copolymer Based Polymer Systems". Beamtime at Daresbury was provided under EPSRC Grant GR/N22052. We are grateful to Dr. J. G. Grossmann and Dr. A. J. Gleeson for assistance with the SAXS experiments.

References and Notes

(1) Ball, P. *Designing the Molecular World*; Princeton University Press: Princeton, 1996.
(2) Fairclough, J. P. A.; Mai, S.-M.; Matsen, M. W.; Bras, W.; Messe, L.; Turner, S.; Gleeson, A. J.; Booth, C.; Hamley, I. W.; Ryan, A. J. *J. Chem. Phys.* **2001**, *114*, 5425.
(3) Hamley, I. W. *The Physics of Block Copolymers*; Oxford University Press: Oxford, 1998.
(4) Hamley, I. W. *Adv. Polym. Sci.* **1999**, *148*, 113.
(5) Séguéla, R.; Prud'homme, J. *Polymer* **1989**, *30*, 1446.
(6) Kofinas, P.; Cohen, R. E. *Macromolecules* **1994**, *27*, 3002.
(7) Hamley, I. W.; Fairclough, J. P. A.; Terrill, N. J.; Ryan, A. J.; Lipic, P. M.; Bates, F. S.; Towns-Andrews, E. *Macromolecules* **1996**, *29*, 8835.
(8) Hamley, I. W.; Fairclough, J. P. A.; Ryan, A. J.; Bates, F. S.; Towns-Andrews, E. *Polymer* **1996**, *37*, 4425.
(9) Ryan, A. J.; Hamley, I. W.; Bras, W.; Bates, F. S. *Macromolecules* **1995**, *28*, 3860.
(10) Loo, Y.-L.; Register, R. A.; Ryan, A. J. *Phys. Rev. Lett.* **2000**, *84*, 4120.
(11) Loo, Y.-L.; Register, R. A.; Adamson, D. H. *Macromolecules* **2000**, *33*, 8361.
(12) Zhu, L.; Cheng, S. Z. D.; Calhoun, B. H.; Ge, Q.; Quirk, R. P.; Thomas, E. L.; Hsiao, B. S.; Yeh, F.; Lotz, B. *J. Am. Chem. Soc.* **2000**, *122*, 5957.
(13) Zhu, L.; Huang, P.; Cheng, S. Z. D.; Ge, Q.; Quirk, R. P.; Thomas, E. L.; Lotz, B.; Wittmann, J.-C.; Hsiao, B. S.; Yeh, F.; Liu, L. *Phys. Rev. Lett.* **2001**, *86*, 6030.
(14) Zhu, L.; Mimnaugh, B. R.; Ge, Q.; Quirk, R. P.; Cheng, S. Z. D.; Thomas, E. L.; Lotz, B.; Hsiao, B. S.; Yeh, F.; Liu, L. *Polymer* **2001**, *42*, 9121.
(15) Zhu, L.; Calhoun, B. H.; Ge, Q.; Quirk, R. P.; Cheng, S. Z. D.; Thomas, E. L.; Hsiao, B. S.; Yeh, F.; Liu, L.; Lotz, B. *Macromolecules* **2001**, *34*, 1244.
(16) Zhu, L.; Cheng, S. Z. D.; Calhoun, B. H.; Ge, Q.; Quirk, R. P.; Thomas, E. L.; Hsiao, B. S.; Yeh, F.; Lotz, B. *Polymer* **2001**, *42*, 5829.
(17) Zhu, L.; Huang, P.; Chen, W. Y.; Ge, Q.; Quirk, R. P.; Cheng, S. Z. D.; Thomas, E. L.; Lotz, B.; Hsiao, B. S.; Yeh, F.; Liu, L. *Macromolecules* **2002**, *35*, 3553.
(18) Huang, P.; Zhu, L.; Cheng, S. Z. D.; Ge, Q.; Quirk, R. P.; Thomas, E. L.; Lotz, B.; Hsiao, B. S.; Liu, L.; Yeh, F. *Macromolecules* **2001**, *34*, 6649.
(19) Quiram, D. J.; Register, R. A.; Marchand, G. R.; Ryan, A. J. *Macromolecules* **1997**, *30*, 8338.
(20) Quiram, D. J.; Register, R. A.; Marchand, G. R.; Adamson, D. H. *Macromolecules* **1998**, *31*, 4891.
(21) Nojima, S.; Kato, K.; Yamamoto, S.; Ashida, T. *Macromolecules* **1992**, *25*, 2237.
(22) Rangarajan, P.; Register, R. A.; Fetters, L. J.; Bras, W.; Naylor, S.; Ryan, A. J. *Macromolecules* **1995**, *28*, 4932.
(23) Rohadi, A.; Endo, R.; Tanimoto, S.; Sasaki, S.; Nojima, S. *Polym. J.* **2000**, *32*, 602.
(24) Quiram, D. J.; Register, R. A.; Marchand, G. R. *Macromolecules* **1997**, *30*, 4551.
(25) Vigild, M. E.; Almdal, K.; Mortensen, K.; Hamley, I. W.; Fairclough, J. P. A.; Ryan, A. J. *Macromolecules* **1998**, *31*, 5702.
(26) Ryan, A. J.; Fairclough, J. P. A.; Hamley, I. W.; Mai, S.-M.; Booth, C. *Macromolecules* **1997**, *30*, 1723.
(27) Floudas, G.; Ulrich, R.; Wiesner, U. *J. Chem. Phys.* **1999**, *110*, 652.
(28) Floudas, G.; Ulrich, R.; Wiesner, U.; Chu, B. *Europhys. Lett.* **2000**, *50*, 182.
(29) Floudas, G.; Vazaiou, B.; Schipper, F.; Ulrich, R.; Wiesner, U.; Iatrou, H.; Hadjichristidis, N. *Macromolecules* **2001**, *34*, 2947.
(30) Towns-Andrews, E.; Berry, A.; Bordas, J.; Mant, G. R.; Murray, P. K.; Roberts, K.; Sumner, I.; Worgan, J. S.; Lewis, R.; Gabriel, A. *Rev. Sci. Instrum.* **1989**, *60*, 2346.
(31) Bliss, N.; Bordas, J.; Fell, B. D.; Harris, N. W.; Helsby, W. I.; Mant, G. R.; Smith, W.; Towns-Andrews, E. *Rev. Sci. Instrum.* **1995**, *66*, 1311.
(32) Pople, J. A.; Hamley, I. W.; Fairclough, J. P. A.; Ryan, A. J.; Komanschek, B. U.; Gleeson, A. J.; Yu, G.-E.; Booth, C. *Macromolecules* **1997**, *30*, 5721.
(33) Hamley, I. W.; Pople, J. A.; Gleeson, A. J.; Komanschek, B. U.; Towns-Andrews, E. *J. Appl. Crystallogr.* **1998**, *31*, 881.
(34) Almdal, K.; Bates, F. S.; Mortensen, K. *J. Chem. Phys.* **1992**, *96*, 9122.
(35) Koppi, K. A.; Tirrell, M.; Bates, F. S.; Almdal, K.; Mortensen, K. *J. Rheol.* **1994**, *38*, 999.
(36) Hamley, I. W. *J. Phys.: Condens. Matter* **2001**, *13*, R643.

(37) Schulz, M. F.; Bates, F. S.; Almdal, K.; Mortensen, K. *Phys. Rev. Lett.* **1994**, *73*, 86.
(38) Zhao, J.; Majumdar, B.; Schulz, M. F.; Bates, F. S.; Almdal, K.; Mortensen, K.; Hajduk, D. A.; Gruner, S. M. *Macromolecules* **1996**, *29*, 1204.
(39) Floudas, G.; Hilliou, L.; Lellinger, D.; Alig, I. *Macromolecules* **2000**, *33*, 6466.
(40) Floudas, G.; Schipper, F.; Castelletto, V.; Hamley, I. W. Manuscript in preparation.
(41) Mai, S.-M.; Fairclough, J. P. A.; Terrill, N. J.; Turner, S. C.; Hamley, I. W.; Matsen, M. W.; Ryan, A. J.; Booth, C. *Macromolecules* **1998**, *31*, 8110.
(42) Rançon, Y.; Charvolin, J. *J. Phys. Chem.* **1988**, *92*, 2646.
(43) Clerc, M.; Levelut, A. M.; Sadoc, J. F. *J. Phys. II* **1991**, *1*, 1263.

MA0207069